Northwest Atlantic Fisheries Organization

Interannual Variabilities in the Arctic Ice Cover, Labrador Sea Salinity

and Labrador Shelf Ice Cover

by

M. Ikeda

Physical and Chemical Sciences, Department of Fisheries and Oceans
BIO, P. O. Box 1006, Dartmouth, Nova Scotia, Canada B2Y 4A2

Feedback mechanisms among decadal oscillations of northern hemisphere atmospheric circulation, Arctic-subarctic ice cover and ocean circulation are studied. Decadal oscillations of Arctic-subarctic ice cover have been observed, most significantly in the Barents Sea and Labrador Shelf. The extreme southward extent of Labrador ice is explained by local weather conditions such as low air temperatures and strong northwesterly winds. This weather pattern is attributed to atmospheric circulation with low pressure anomalies in the Arctic. Barents Sea ice has weak correlation with local air temperature but is highly correlated with this atmospheric circulation. Cyclonic wind stress curl associated with the atmospheric circulation plays a role to exchange cold Arctic water and warm Atlantic water in the Arctic-Atlantic system and reduces Barents Sea ice. More heat flux from the Barents Sea with less ice to the atmosphere tends to produce low pressure in the Arctic. This positive feedback amplifies the oscillations of the air-ice-ocean system forced by solar activity with a relatively weak variability. A simple numerical model of ocean circulation suggests that a response amplitude has a peak at a decadal time scale.

Ice cover

Monthly anomalies of areal sea ice extent are taken from Mysak and Manak (1988) and plotted in Fig.1 for the entire Arctic and three regions; Barents Sea, Greenland Sea and Baffin Bay/Labrador Sea. The anomalies have been smoothed by applying 25-month running mean. Clear decadal oscillations are seen in Barents Sea and Baffin Bay/Labrador Sea. In the entire Arctic, the ice extnet has a dominant peak in 1966-1970 about a decade after the peak in 1956-1957. However, ice has decayed after 1970 without a clear peak around 1980. Greenland Sea ice has one distinguished peak around 1968. The anomalies of sea ice extent south of 55°N over the Labrador Shelf in March also are shown in Fig.1 (Ikeda et al., 1988). Although the data is short, decadal oscillations are evident.

Air temperature

Annual air temperature in the entire Arctic and three regions are taken from Kelly et al. (1982) and shown in Fig.2. Since quasi- biennial oscillations are comparable with and mask the longer-period oscillations, a two-year filter is applied to the annual temperature as follows:

$$T'_n = (T_{n-1} + 2T_n + T_{n+1}) / 4 \qquad (1)$$

where T is an origianl temperature, T' is a filtered value, and the suffix n denotes a year. Air temperature at Battle Harbour (52°N, Labrador coast) in January and February is shown in Fig.2. The general trend in the Arctic is cooling from 1950 to 1970, followed by gentle warming. Superimposed upon this trend, decadal oscillations are seen in the total Arctic with temperature minima around 1956 and 1965. Significant features in the Barents Sea and Greenland Sea are temperature minima around 1968. Decadal oscillations are visible in the Labrador coastal temperature.

SPECIAL SESSION ON ENVIRONMENTAL CONDITIONS

Atmospheric circulation
    Atmospheric pressure at the sea surface has been analyzed by Trenberth
and Paolino (1981), using empirical orthogonal function (EOF) analysis. The
first EOF of the annual mean pressure field is shown in Fig.3. The first EOF,
which explains about 20% of variance (mb^2), has a low anomaly in the Arctic
and two high anomalies over the Pacific and Europe. The time series smoothed
by the two-year filter exhibits decadal oscillations with positive values in
the three periods, 1953-55, 1962-65 and 1972-76, corresponding to 0.5-1.5mb
low anomalies in the Arctic. The atmospheric circulation associated with this
pressure field intensifies westerly winds in the subarctic. Due to its
meridional component, it contributes to northwesterly winds over Labrador and
southwesterly winds in the Greenland Sea. Note that the circulation produces
cyclonic wind stress curl in the Barents Sea.

Relationship among ice cover, air temperature and atmospheric circulation
(a) ice cover-air temperature
    Although the icreases in entire Arctic ice cover in 1956-57 and 1964-66
are explained by low air temperature, no explantion is provided for the
reduction of ice and low air temperature in 1970-75. There is clear inverse
correlation between Barents Sea ice and air temperature after 1966, whereas
ice variability before 1966 is not explained by air temperature. The
better inverse correlation is found for the Greenland Sea and Baffin Bay/
Labrador Sea. The variabilities in Labrador ice cover south of 55°N are well
correlated with air temperature at Battle Harbour. This correlation has been
reproduced by a numerical sea ice model, not only qualitatively but also
quantitatively (Ikeda et al., 1988).

(b) air temperature-atmospheric circulation
    The air temperature at Battle Harbour is highly correlated with the first
EOF of the air pressure field. Correlation between the first EOF and air
temperature in the other regions is low.

(c) ice cover-atmospheric circulation
    Since the decadal oscillations have been found in Barents Sea ice and the
first EOF of the atmospheric pressure field, mechanisms of the link between
these two variables are seeked. The low pressure anomaly in the Arctic tends
to produce cyclonic wind stress curl over the Barents Sea and Fram Strait
area. Cyclonic ocean circulation generated by the wind stress curl takes a
role to exchange cold Arctic water with sea ice and warm Atlantic water
through the Fram Strait and Barents Sea. Thus, low pressure anomalies in the
Arctic tends to reduce Barents Sea ice. Quantitative discussion will be given
in a section of ocean modelling and show that the wind stress variabilities
can produce the variabilities in ice cover.
    A feedback mechanism from ice cover to atmospheric circulation is
discussed next. Since no study has been done directly for this feedback, a
study of feedback from open ocean to atmosphere by Egger (1977) is referred
to. Extra heat flux of ~50Wm^{-2}, which is supplied by 1°C higher sea surface
temperature, with an area of $3 \times 10^6 km^2$ for 1 month produces a low atmospheric
pressure anomaly of 3mb. In the subarctic winter, an open ocean is estimated
to supply additional heat flux to atmosphere by 200-300Wm^{-2} relative to the
ice-covered sea surface. An extra ice-free area of $2 \times 10^5 km^2$ in the Barents
Sea for 3 months gives heat flux equivalent to that of Egger's model. Thus, a
low pressure anomaly by 3mb in winter or 1mb in the annual mean can be
attributed to the ice-free area in the Barents Sea.

    Consideration of relationship among the three variables leads to the
following suggestion: the northern hemisphere atmospheric circulation
determines local weather of Labrador, and then, low air temperature increases
sea ice over the Labrador Shelf. Feedback mechanisms are expected between the
atmospheric circulation and ice in the Arctic, particularly the Barents Sea.
Cyclonic wind stress curl over the Barents Sea and Fram Strait, associated
with the low atmospheric pressure in the Arctic, tends to reduce Barents Sea
ice, and in turn, more open water in the Barents Sea generates the low
pressure in the Arctic. This cause-results relationship is shown in Fig.4.

Other parameters
(a) sunspot
    It is well known that the number of sunspots has decadal oscillations.
The annual mean Zurich sunspot numbers are taken from Paine (1983) and plotted
in Fig.5. The sunspots were fewer in 1952-55, 1963-66 and 1974-76, when the
low pressure anomalies in the Arctic developed. The total solar radiation
energy varies only by one-tenth percent, whereas enrgy spectra vary

significantly so that the vertical profile of heating shows an ~ 10%
variability (Paine, 1983). During the fewer sunspot periods, a temperature
gradient in the stratosphere was intensified and stabilizes the stratosphere.
The more stable atmosphere is predicted to have intensified circulation.
However, it is doubtful that this weak variability in solar activity can cause
the atmospheric circulation anomalies (Kerr, 1982). Hence, positive feedback,
by which responses of atmosphere-ocean system are amplified, is required
between the atmosphere and ocean.

(b) ocean temperature and salinity
       Nine Ocean Weather Stations in the North Atlantic show no clear decadal
oscillation (Taylor and Stephens, 1980). Reduction of salinity at OWS Bravo
in the Labrador Sea in 1968-71 might be related to fresh water flowing from
the Arctic after anomalous ice melt (Ikeda, 1987).

(c) Soviet river discharge
       It might be expected that heavier ice in the Barents Sea was caused by
more discharge from Soviet rivers. However, the discharge shows no decadal
oscillation (Cattle, 1985).

A numerical ocean model
(a) necessity of the ocean model
       The above discussion of the decadal oscillations of various parameters
leads to a study of feedback mechanisms between the atmosphere and ocean
(including ice), because a variability of solar activity, which is external
forcing for the atmosphere-ocean system, can not solely produce the observed
variability of atmospheric circulation without positive feedback. Further
consideration convinces us that the positive feedback is necessary but not
enough. To produce dominant decadal oscillations of the atmosphere-ocean
system, the external forcing has to have a dominant decadal oscillation among
various oscillations. The other case is that the atmosphere-ocean system
responds to the external forcing with a maximum amplitude at a decadal time
scale. The maximum response becomes possible when the ocean has an
oscillatory response to a sudden change in the atmosphere. It is unrealistic
that atmospheric responses are oscillatory with a decadal time scale, because
the atmosphere responds at much shorter (a month at longest) time scales. In
this paper, a maximum oceanic response to the atmosphere is investigated.
       According to Semtner (1987), the upper 100-200m layer of the Arctic water
circulates anticyclonically in Canadian Basin and flows out from Eurasian
Basin to the Atlantic through the Fram Strait. The Atlantic water enters the
Arctic in the lower layer as well as through the Barents Sea. As suggested by
a wind- and buoyancy-driven two-level model developed by Ikeda (1987),
buoyancy-driven flow, which is similar to the Arctic-Atlantic water exchange,
shows an oscillatory response to sudden change in wind stress curl.

(b) model description
       The two-level model used in this paper is similar to that in Ikeda
(1987). The model has a rigid lid and a friction less, flat bottom in a
rectangular closed domain on a β-plane. Hydrostatic and Boussinesq
approximations are used, and nonlinear advection terms are omitted in the
momentum equations. The velocity field can be decomposed into barotropic and
baroclinic components. The barotropic component is purely driven by wind
stress without feedback from the baroclinic component. The wind stress is
assumed to determine Ekman transport uniquely and be zonal with a linear
meridional gradient and zero at the center. The zonal barotropic momentum
equation is assumed to be in geostrophic balance, while acceleration and
horizontal viscous terms are retained in the meridional barotropic momentum
equation. Sverdrup balance holds in the eastern domain, while a narrow
western boundary current exists with the no-slip boundary condition.
       The momentum equations for the baroclinic component are simplified from
those in Ikeda (1987). Ikeda retained acceleration and horizontal viscous
terms in the meridional equation, whereas, in this paper, a geostrophic
balance is assumed in both zonal and meridional directions. The geostrophic
balance rules out an internal Kelvin wave propagating along the eastern and
western boundaries. However, the model in this paper, in which no flow normal
to the boundaries is assumed similar to Ikeda (1987), reproduces propagation
of a density anomaly along the boundaries within 10% differences. .
       The density equations have nonlinear advection terms and horizontal and
vertical diffusion terms. To simulate buoyancy-driven circulation in the
Arctic-Atlantic, buoyancy and density (negative buoyancy) are given in the
northern and southern portions, respectively. The buoyancy and density fluxes

are represented by the right-hand-side term in the density equations,

$$M_j(\rho_j^* - \rho_j)/h_i, \qquad (j = 1, 2) \qquad\qquad (2)$$

where

$\rho_1^* = \rho_0 - 1 \ (kg \ m^{-3})$ $\rho_2 = \rho_0 - 0.25$ for buoyancy flux in north

$M_j = 0$ for no flux in middle

$\rho_1 = \rho_0 - 0$ $\rho_2 = \rho_0 + 0.25$ for density flux in south

ρ denotes density, h is a level thickness, M is a volume exchange rate between the model and exterior, the suffixes 1 and 2 denote the upper and lower levels, respectively, and ρ_0 is the reference density, which is equal to the initial lower level density.

A simple idealized model domain is used in this paper, because the purpose is to examine existence of an oscillatory response of the ocean circulation in the area of water exchange between the Arctic and Atlantic. As shown in Fig.6, the rectangular domain resembles Eurasian Basin and some portion of Greenland Basin, in which fresh water flows southward in the upper layer, and more saline water flows northward in the lower layer. Canadian Basin has anticyclonic circulation and supplies relatively fresh water to Eurasian Basin in the upper layer. The circulation pattern in the Arctic is separated by Lomonosov Ridge. Hence, Canadian Basin is excluded from the model but its contribution to fresh water (buoyancy) flux is included. Dominant circulation in the Kara Sea and Barents Sea are cyclonic and separated from the Arctic-Atlantic exchange pattern by islands and shelf break. Thus, the eastern boundary of the model domain is considered to represent condition in the Barents Sea.

The parameters used in this paper are: the upper level thickness is 300m, the lower level thickness is 2700m, the zonal length is 1000km, the meridional length is 2000km, the Coriolis parameter at the center is $1.4\times10^{-4} \ s^{-1}$, its meridional gradient is $0.3\times10^{-11} \ m^{-1}s^{-1}$, a basic density difference between the two levels is $0.5kg \ m^{-3}$, horizontal viscosity and diffusion coefficients are $10^3 \ m^2s^{-1}$, and a vertical diffusion coefficient is $0.5\times10^{-3} \ m^2s^{-1}$. The volume exchange rates are 3Sv and 2Sv for the upper and lower levels respectively, being uniformly distributed in the rectangular domains on the northern and southern boundaries with 300km meridional lengths. The numerical grid size is 25km (zonal) x 100km (meridional). The time step in numerical intgration is taken to be 2 days.

(c) results

The initial density structure in the upper level has uniform low (by -0.25) and high (by 0.25) in the northern and southern portions with 600km meridional lengths connected by a linear gradient. Although an equilibrium state is independent of the initial structure in the upper level, the solution converges faster with this initial condition than it does with a uniform upper level. A calculation is carried out for 18 years with no wind stress to examine convergence to the equilibrium. The solution at t = 18 years is shown in Fig.7, and the evolution is shown in Fig.8 by density structures. The meridional and zonal differences in the vertically integrated density show that the solution converges to the equilibrium with a typical time scale of 3 years. The process occurring until the equilibrium is as follows: zonal geostrophic flow associated with a meridional density gradient is westward and eastward in the upper and lower levels, respectively. Resultant downwelling and upwelling produce low and high density anomalies on the western and eastern boundaries. This zonal density gradient, smoothed by horizontal diffusion, produces southward and northward flows in the upper and lower levels, respectively. The streamfunction in Fig.7 indicates southwestward flow in the upper level and exactly opposite flow in the lower level, where the barotropic component is zero. Thus, the equilibrium of a density balance has been established; i.e., low density water due to the buoyancy flux in the northern portion in the upper level flows southward and downwells in the southern portion, where the density flux increases density of water, which flows northward in the lower level and upwells in the northern portion.

Two additional cases are carried out by applying suddenly imposed steady wind stresses after t = 9 years. One case has cyclonic wind stress, whcih is specified by zonal wind stress $\tau = -0.02y \ 10^{-6} \ Pa \ m^{-2}$, and the other case has anticyclonic wind with a gradient of $0.02 \ Pa \ m^{-3}$. The barotropic wind-driven component is spun up in 100days, whereas a spin-up time for the baroclinic component is much longer. However, horizontal diffusion tends to soomth zonal density gradient so that the baroclinic component, whcih reaches equilibrium in a diffusion time scale of ~ 1 year, is minor. Thus, the circulation

directly driven by wind is nearly barotropic. The cyclonic (anticyclonic) wind stress produces northward (southward) volume transport of ~6 Sv, which satisfies Sverdrup balance in the area 800-900km from the eastern boundary. This meridional flow returns southward (northward) near the western boundary.

The solutions at t - 18 years are shown in Fig.7. The cyclonic wind stress tends to push light water westward in the north of the upper level so that the southward flow is narrowed toward the western boundary. The anticyclonic wind stress carries light water eastward and makes the southward flow shift near the eastern boundary. The flow pattern is not simply linear superposition of the wind-driven flow and buoyancy-driven flow, but the density structure is modified by wind-driven circulation and determines flow pattern. The adjustment takes place within a time scale of 3 years (Fig.8). The meridional density difference and the position of the upper level density of -0.5 overshoot around 2 years after the wind changes and then converge to the equilibrium. The solutions at t - 18 years (9 years after the wind change) enable us to estimate oceanic responses to a variable wind stress with an oscillation period of 9 x 4 ~ 40 years.

Two extra cases with variable wind stresses are carried out. The wind stress curl is specified to be

$$\text{curl } \tau - -\partial \tau / \partial y - 0.02 \sin 2\pi(t-9)/\bar{T} \quad \text{for } t>9 \text{ (years)} \quad (3)$$

where $\bar{T}$ is a period of wind stress oscillation. The wind stress is cyclonic in the first half period, and then it changes to anticyclonic in the second half. One case has $\bar{T}$ - 3 years, and the other case has a 9 years period. The evolutions of the density structures are shown in Fig.8. The 9-year period case produces larger variabilities of meridional density differences than the 3-year period case. The wind stress varies rapidly in the 3-year period case so that the density structures do not adjust to the wind stress. The meridional density differences in the 9-year period case have the peak-to-peak amplitudes larger than those between the two steady wind cases. Thus, the oceanic responses have larger amplitudes with the 9-year period wind than with ~40 year-period winds. This maximum amplitude response occurs because the density structures overshoot before equilibrium is established.

Application to the Barents Sea

The larger zonal density difference in the upper level, associated with higher (lower) density in the eastern (western) half portion, is interpreted to be less ice in the eastern portion of Eurasian and Greenland basins. The northward shift of isopycnal contours is related to less ice in the Barents Sea. Thus, a cyclonic wind stress tends to reduce Barents sea ice. The amplitude of ice variability is a function of a period of wind stress variability. The northward shift of 200km, corresponding to the 9-year period wind, is equivalent to an ice-covered area less by $2 \times 10^5 \text{km}^2$ in the Barents Sea with a 1000km width, and is comparable with the observed variability (Fig.1).

When feedback between wind stress and ice cover is estimated, a phase of an oceanic response should be taken into account, in addition to its amplitude. Responding to the 3-year period wind, the density variabilities have maxima and minima about a quarter of the period later than the maximum and minimum of wind stress curl (Fig.8). Thus, the least and most ice covers occur when wind stress is zero, and the strongest cyclonic and anticyclonic wind stresses correspond to normal ice cover. The 9-year period wind produces maxima and minima of density variability about one-tenth of the period later than the maximum and minimum of wind stress curl; i.e., the least and most ice covers nearly correspond to the strongest cyclonic and anticyclonic wind stresses. The differences in the meridional positions of the -0.5 upper level density between the strongest wind stresses are taken for the three different cases:

0 km for 3-year period, 190 km for 9-year, and 20 km for ~40-year
The zonal density differences show also the largest amplitude with the 9-year period wind variability. These oceanic responses suggest that positive feedback mechanism works most efficiently at decadal time scales.

References

Cattle, H., 1985: Diverting Soviet rivers: some possible repercussions for the Arctic Ocean. Polar Record, 22, 485-498.

Egger, J., 1977: On the linear theory of the atmospheric response to sea surface temperature anomalies. J. Atmos. Sci., 34, 603-614.

Ikeda, M., 1987: Salt and heat balances in the Labrador Sea using a box model. Atmosphere-Ocean, 25, 197-223.

Ikeda, M., 1987: Wind effects on the buoyancy-driven general circulation in a closed basin using a two-level model. J. Phys. Oceanogr., 17, 1707-1723.

Ikeda, M., T. Yao and G. Symonds, 1988: Simulated fluctuations in annual Labrador Sea-ice cover. Atmosphere-Ocean, 26, 16-39.

Kelly, P.M., P.D. Jones, C.B. Sear, B.S.G. Cherry and R.K. Tavakol, 1982: Variations in surface air temperatures: Part 2. Arctic regions, 1881-1980. Mon. Wea. Rev., 110, 71-83.

Kerr, R.A., 1982: Sun, weather, and climate: a connection?. science, 217, 917-919.

Mysak, L.A., and D.K. Manak, 1988: Arctic sea ice extent and anomalies, 1953-1984. Climate Research Group Report, No. 88-8, McGill University.

Paine, D.A., 1983: A climate hypothesis describing the solar-terrestrial system as a frequency domain with specific response characteristics. Trans. AGU, 64, 425-428.

Semtner, A.J., 1987: A numerical study of sea ice and ocean circulation in the Arctic. J. Phys. Oceanogr., 17, 1077-1099.

Taylor, A.H., and J.A. Stephens, 1980: Seasonal and year-to-year variations in surface salinity at the nine North-Atlantic Ocean Weather Stations. Oceanol. Acta, 3, 421-430.

Trenberth, K.V., and D.A. Paolino, 1981: Characteristic patterns of variability of sea level pressure in the northern hemisphere. Mon. Wea. Rev., 109, 1169-1189.
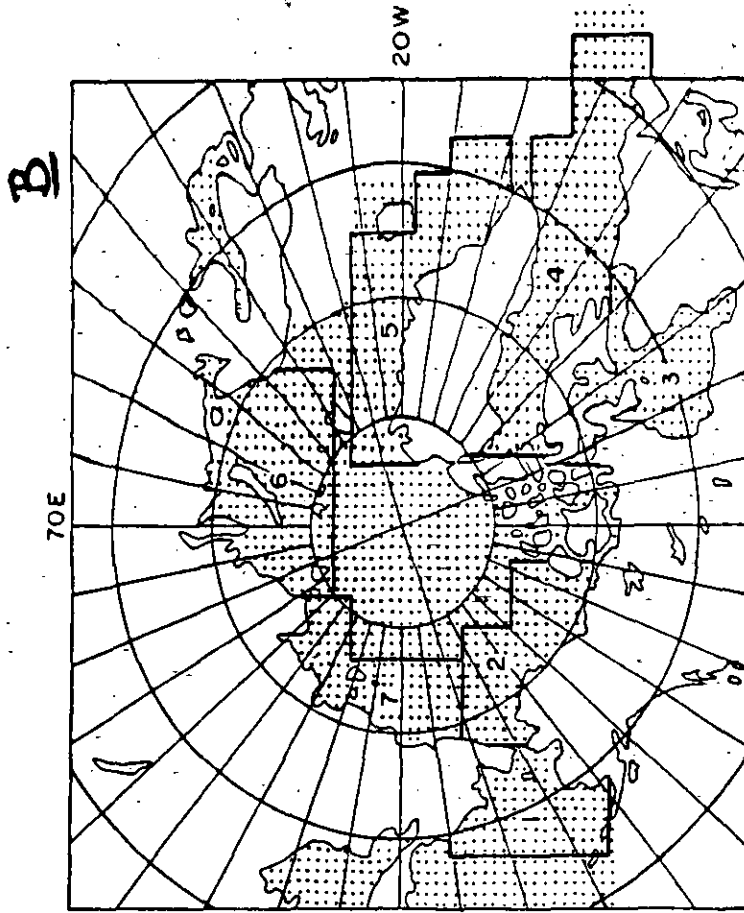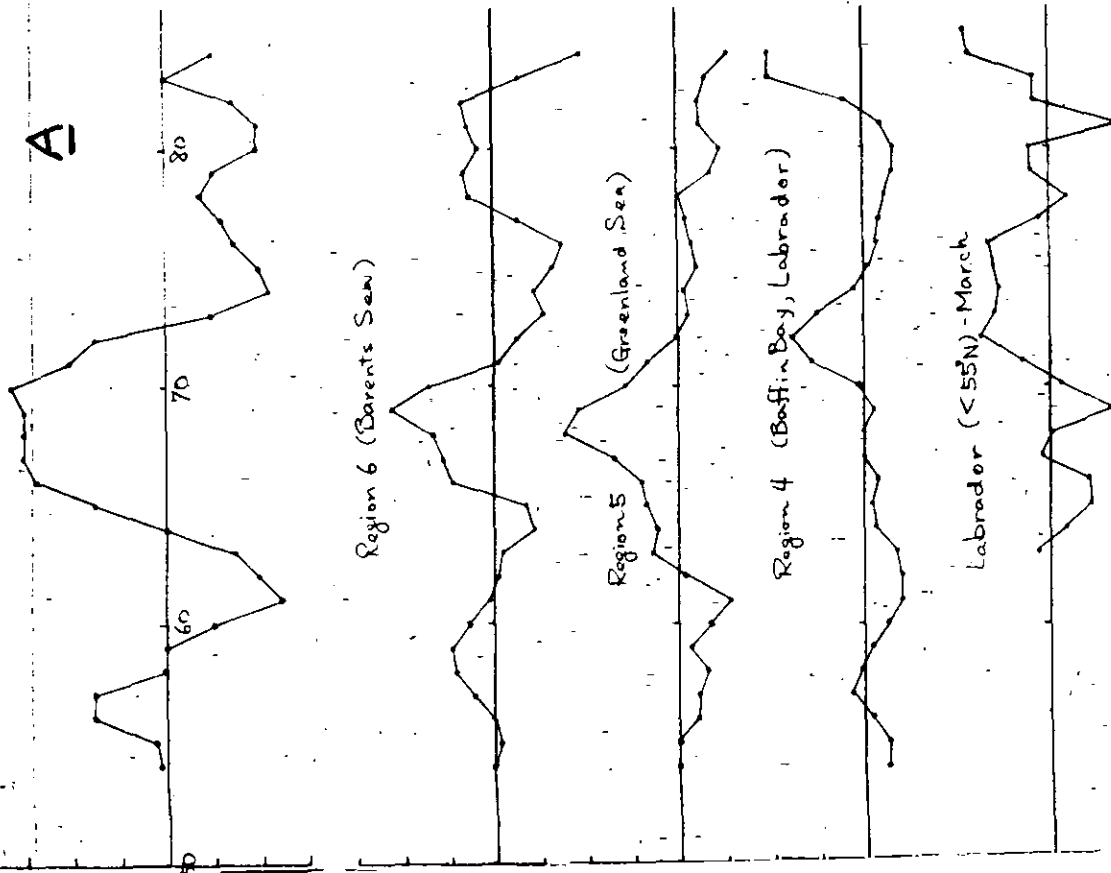
Fig. 1 **A** Monthly anomalies of areal sea ice extent in the total Arctic and three regions defined in **B** along with March anomalies south of 55°N over the Labrador Shelf. The first four data have been reproduced from Mysak and Manak (1988).
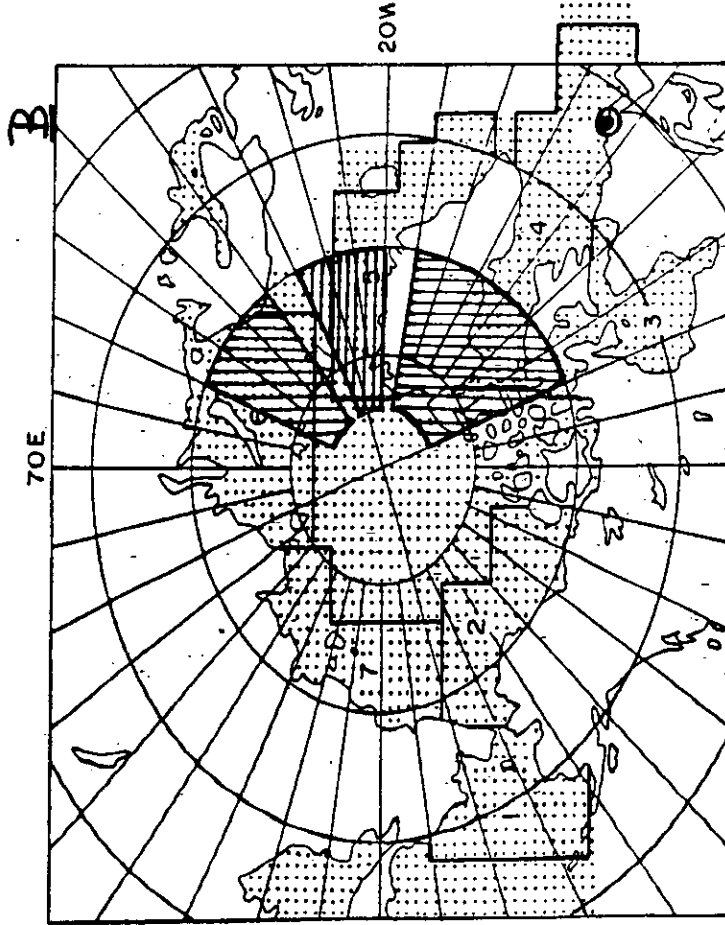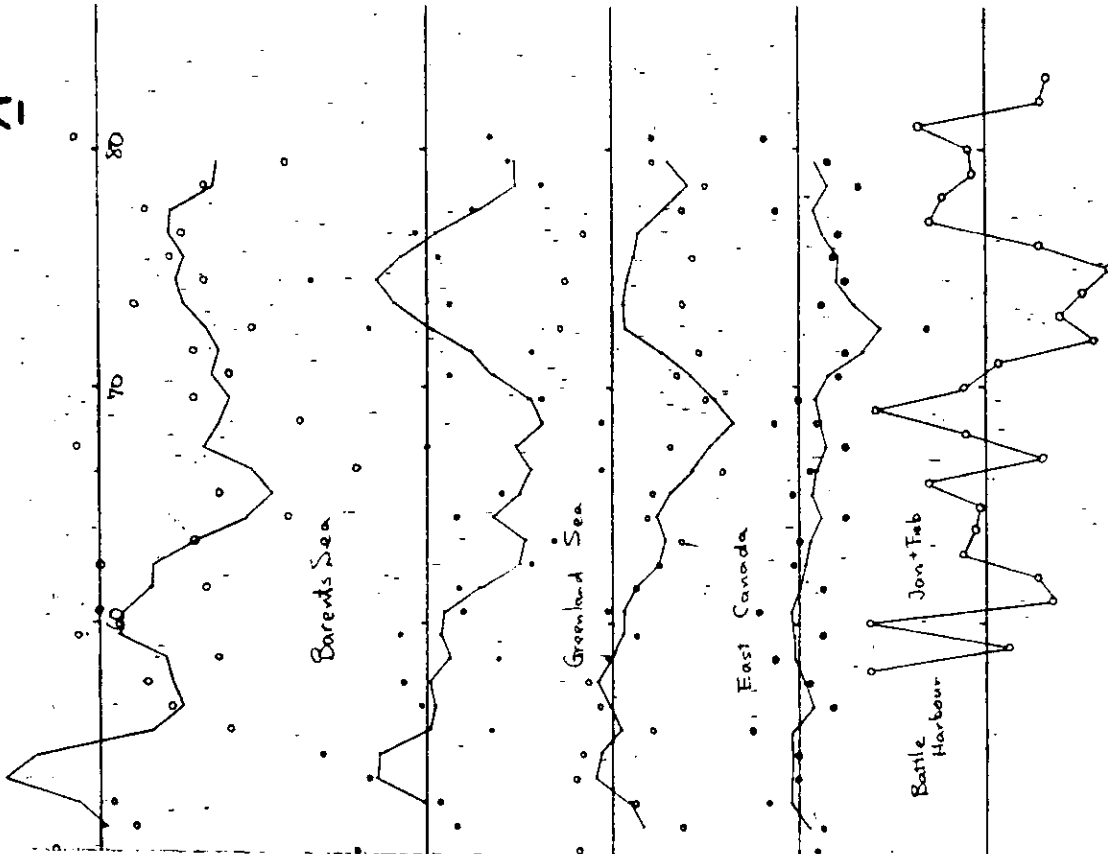
Fig.2 A. Annual air temperature in the Arctic (65-85°N), Barents Sea (70-85°N, 20-50°E), Greenland Sea (70-85°N, 10°E-20°W), and Greenland/Eastern Canada (70-85°N, 30-90°W), whose regions are indicated in B, along with air temperature at (55°N, 55°W) in January and February. The annual data have been reproduced based on Kelly et al. (1982). The original values are shown by dots in addition to the lines of the values smoothed by a two-year filter.
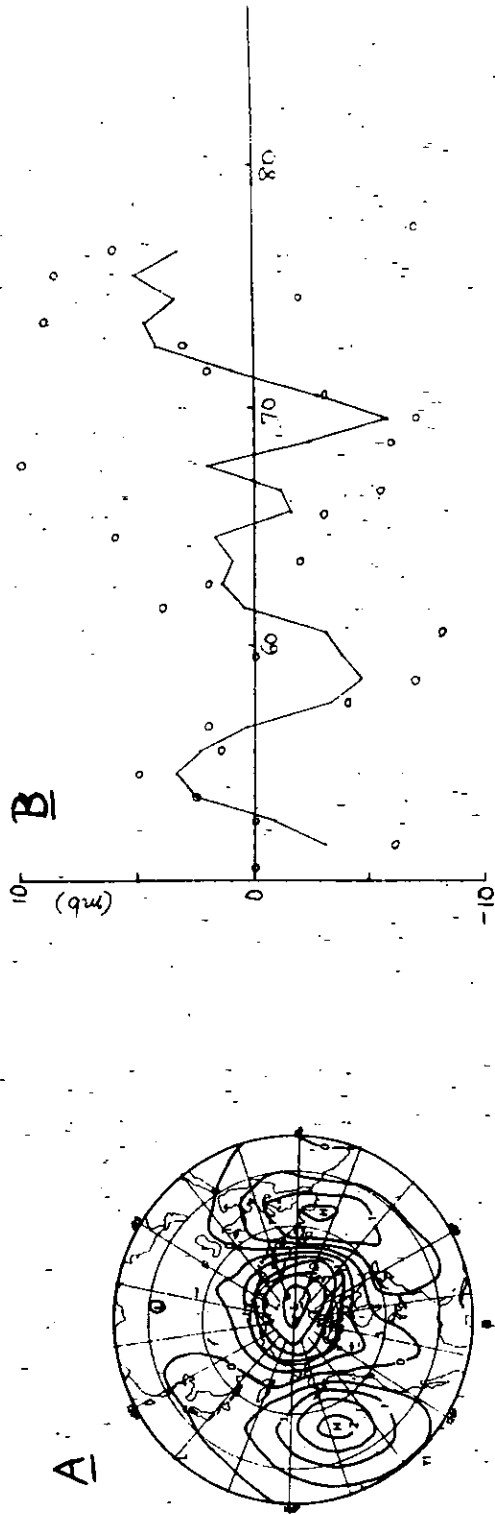
Fig.3 **A** The first empirical orthogonal function of annual mean atmospheric pressure at sea level taken from Trenberth and Paolino (1981), and **B** its time series (open circles) along with the two-year filtered time series.
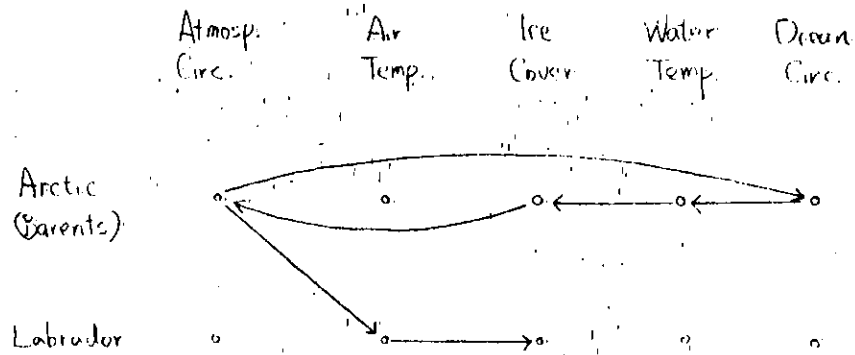
Fig.4 The cause-result relationship among various parameters in the Arctic and Labrador.
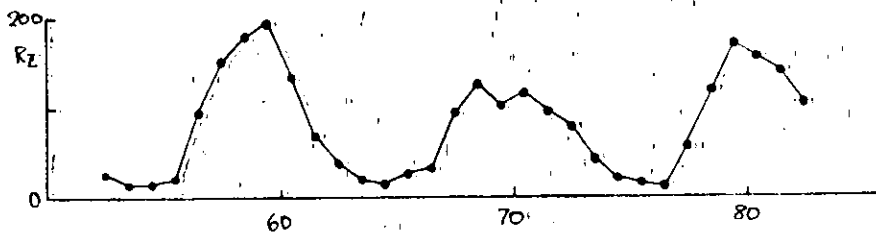
Fig..5 Zurich sunspot. numbers taken from Paine (1983)..
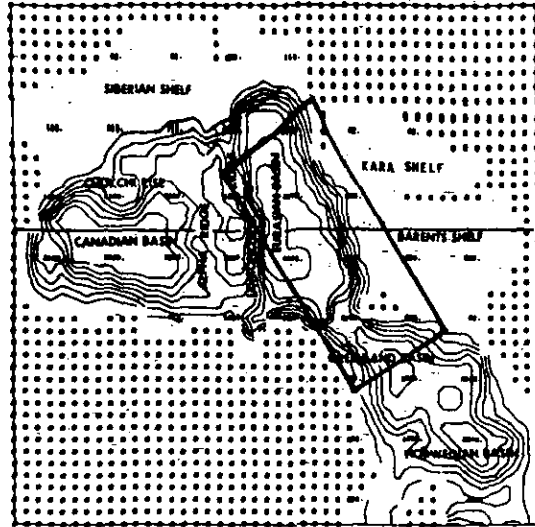
Fig.6 The rectangular model domain used in this paper is superimposed on a bathymetry map.
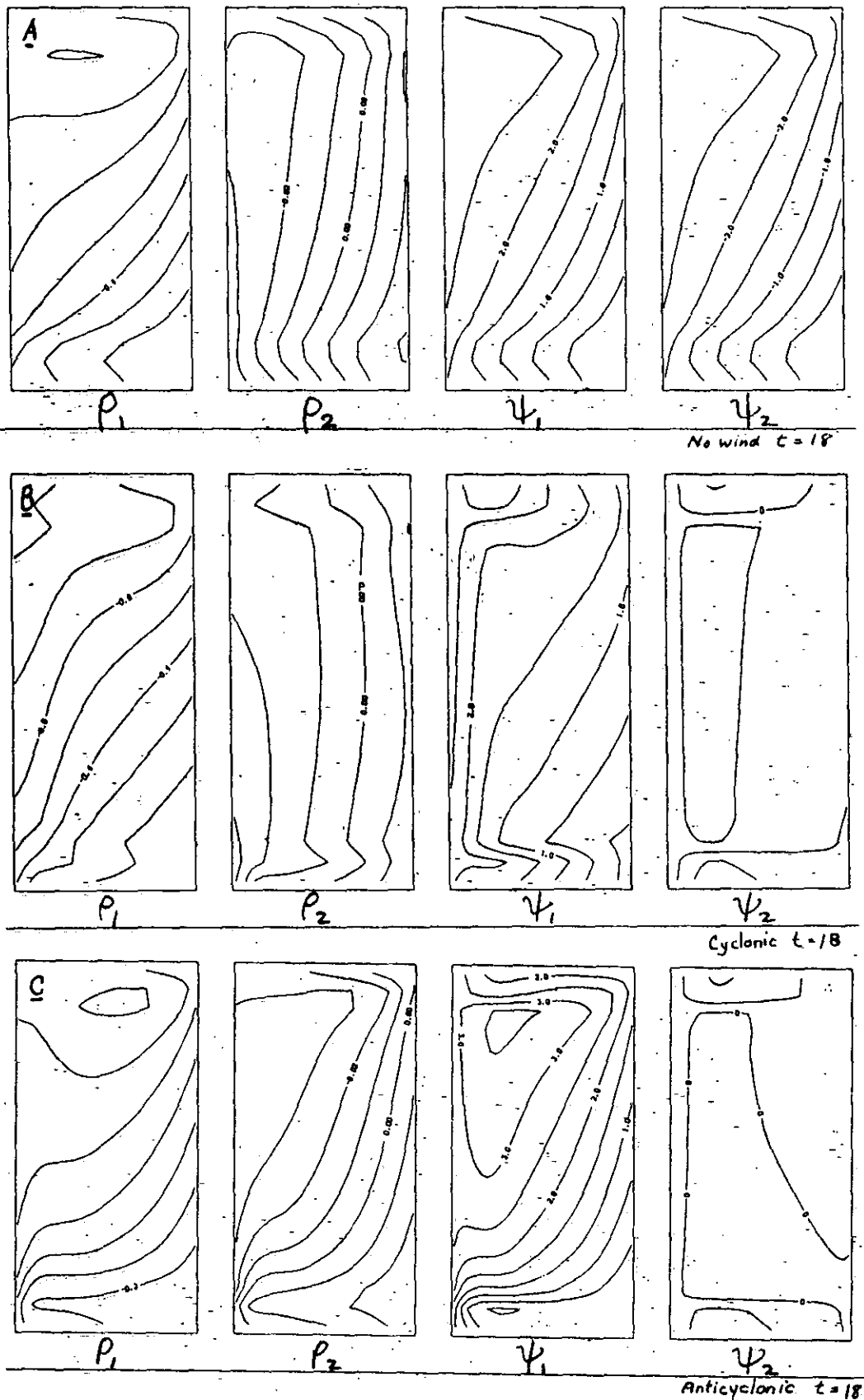
Fig.7 The upper level density, lower level density, upper level
streamfunction and lower level streamfunction at t = 18 years for $\underline{A}$ no wind,
$\underline{B}$ cyclonic wind and $\underline{C}$ anticyclonic wind cases, where Ψ denotes the
streamfunction. The streamfunctions are defined to be

$$\Psi_1 = h_1 \Psi - gh_1 h_2 \rho_A/(2\rho_0 f) \text{ and } \Psi_2 = h_2 \Psi + gh_1 h_2 \rho_A/(2\rho_0 f),$$ where g is the

gravitational acceleration, and Ψ is an approximated barotropic
streamfunction, which is given by integration of the meridional barotropic
volume transport. The contour intervals are 0.1 kg m^{-3} and 0.01 kg m^{-3} for
the upper and lower level densities, and 0.5 Sv for the streamfunctions except
for the lower level streamfunctions in $\underline{B}$ and $\underline{C}$, which have 5 Sv intervals.
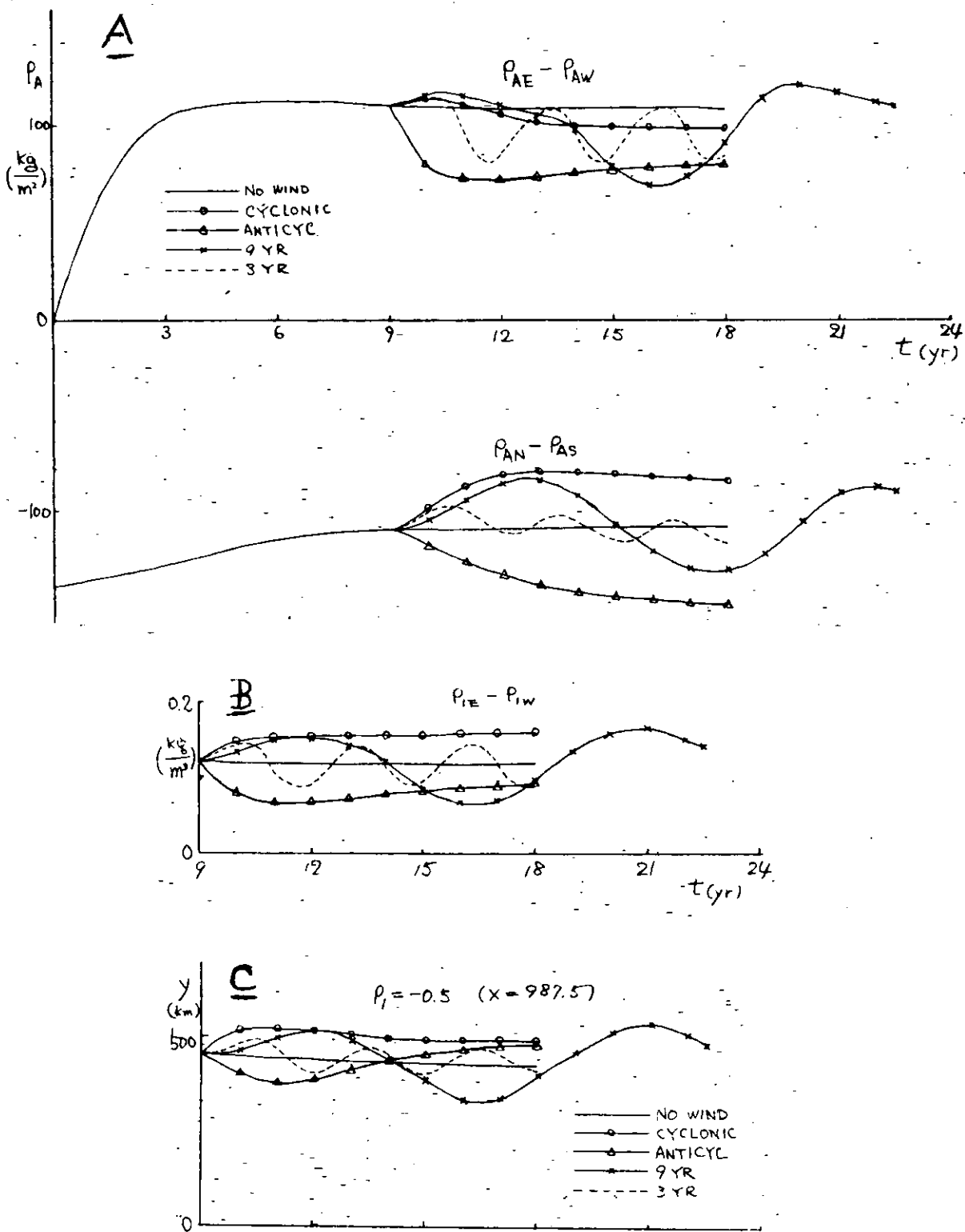
Fig.8 The evolutions of **A** zonal and meridional differences in the
vertically integrated density **B** zonal density difference and **C** meridional
position of the upper level density of -0.5 at the eastmost numerical grids.
The suffix A denotes vertical integration, and N, S, E and W denots the
averages in the northern, southern, eastern and western half portions,
respectively.